Impact of International Shipping Emissions on Ozone and $PM_{2.5}$ in East Asia during Summer: The Important Role of HONO and $ClNO_2$

Jianing Dai[1], **Tao Wang**[1]

Department of Civil and Environmental Engineering, The Hong Kong Polytechnic University, Hong Kong, 999077, China

Correspondence to: Tao Wang (cetwang@polyu.edu.hk)

Abstract. Ocean-going ships emit large amounts of air pollutants such as nitrogen oxide (NO_x) and particulate matter. Ship-released NO_x can be converted to nitrous acid (HONO) and nitryl chloride ($ClNO_2$), which produce hydroxyl (OH) and chlorine (Cl) radicals and recycle NO_x, thus affecting the oxidative capacity and production of secondary pollutants. However, these effects have not been quantified in previous investigations of the impacts of ship emissions. In this study, a regional transport model (WRF–Chem) revised to incorporate the latest HONO and $ClNO_2$ processes was used to investigate their effects on the concentrations of RO_x (RO_2+HO_2+OH) radicals, O_3, and fine particulate matter ($PM_{2.5}$) in Asia during summer. The results show that the ship-derived HONO and $ClNO_2$ increased the concentration of RO_x radicals by approximately two to three times in the marine boundary layer. The enhanced radicals then increased the O_3 and $PM_{2.5}$ concentrations in marine areas, with the ship contributions increasing from 9% to 21% and from 7% to 10%, respectively. The largest RO_x enhancement was simulated over the remote ocean with the ship contribution increasing from 29% to 50%, which led to increases in ship-contributed O_3 and $PM_{2.5}$ from 21% to 38% and from 13% to 19%, respectively. In coastal cities, the enhanced levels of radicals also increased the maximum O_3 and averaged $PM_{2.5}$ concentrations from 5% to 11% and from 4% to 8% to 4% to 12%, respectively. These findings indicate that modeling studies without considering HONO and $ClNO_2$ can significantly underestimate the impact of ship emissions on radicals and secondary pollutants. It is therefore important that these nitrogen compounds be included in future models of the impact of ship emissions on air quality.

1 Introduction

Exhaust emissions by ocean-going ships affect the chemical compositions of the marine atmosphere and have a significant impact on the climate, air quality, and human health (Eyring et al., 2010, Liu et al., 2016, Corbett et al., 2007, Andersson et al., 2009). The key air pollutants emitted by ship vessels include gases such as sulfur dioxide (SO_2) and nitrogen oxides (NO_x = NO + NO_2) and particulate matter (PM) (Eyring et al., 2005, Moldanová et al., 2009). Emissions of NO_x and other ozone (O_3) precursors (volatile organic compounds (VOCs) and carbon monoxide (CO)) from shipping contribute to the tropospheric O_3 burden and hydroxyl radicals (OH), thereby influencing global radiative forcing and oxidative power (Lawrence and Crutzen, 1999). Ship-generated aerosols also affect the radiative budget by scattering and absorbing solar and thermal radiation directly and by altering cloud properties (Eyring et al., 2010, Fuglestvedt et al., 2009, Lawrence and Crutzen, 1999, Liu et al., 2016, Devasthale et al., 2006). Ship emissions in ports and near the coast also influence the air quality of coastal cities (Zhang et al., 2017c, Liu et al., 2018) and threaten public health (Liu et al., 2016, Campling et al., 2013). As international shipborne trade continues to increase, ship emissions are expected to continuously grow at a rate of 3.5% over the 2019-2024 period (UNCTAD, 2019), and their impact on the environment is a growing concern.

The effects of ship emissions on the formation of O_3 and $PM_{2.5}$ have been extensively evaluated in numerical studies. On the open ocean, ship-generated NO_x reacts with VOCs emitted from ships and from the background atmosphere and enhances O_3 formation (Corbett and Fischbeck, 1997, Lawrence and Crutzen, 1999, Aksoyoglu et al., 2016, Huszar et al., 2010, Hoor et al., 2009). In coastal areas, the O_3 levels can also be increased by NO_x emitted from ships in ports and harbors and through the dispersion of ship-formed O_3 on the open ocean (Wang et al., 2019, Aksoyoglu et al., 2016, Song et al., 2010). On the other hand, ship-generated NO_x can reduce ozone formation via a titration effect in heavy-traffic ports and within the ship tracks (Wang et al., 2019, Aksoyoglu et al., 2016). Ship emissions have also been shown to increase $PM_{2.5}$ concentrations via direct emissions and via the production of secondary aerosols through the reaction of gaseous precursors (Aksoyoglu et al., 2016, Liu et al., 2018, Lv et al., 2018). Although the formation of O_3 and secondary aerosols is affected by their precursors, it can also

be influenced by the levels of radicals, which are key to the oxidation of precursors. Limited attention has been paid to the production of ship-related radicals in evaluating the effects of ship emissions on secondary pollutants.

Recent studies have demonstrated the potentially important roles of two radical precursors and nitrogen reservoirs—nitrous acid (HONO) and nitryl chloride ($ClNO_2$)—in the atmospheric oxidation chemistry (Fu et al., 2019, Li et al., 2016, Sarwar et al., 2014, Simon et al., 2009, Zhang et al., 2017a). HONO is emitted directly in combustion and soil (Kleffmann et al., 2005) or produced by heterogeneous reactions of NO_2 on various surfaces (Finlayson-Pitts et al., 2003, Ndour et al., 2008, Monge et al., 2010) and by photolysis of nitrate aerosol (Ye et al., 2017, Ye et al., 2016). $ClNO_2$ is formed from reactions of N_2O_5, which is produced when NO_2 reacts with O_3, on chloride-containing aerosol at night (Bertram and Thornton, 2009). Photolysis of HONO and $ClNO_2$ by sunlight produces OH or Cl radicals and recycles NO_2, hence affecting the oxidation capacity and production of secondary pollutants (Osthoff et al., 2008, Wang et al., 2016). Ships can directly emit HONO (Sun et al., 2020), and their emitted NO_x can produce HONO and $ClNO_2$ via heterogeneous reactions on sea-salt and ship-emitted particles. Although the production and effects of HONO and $ClNO_2$ from land-based emissions have been demonstrated over land areas (Zhang et al., 2017a), few studies have examined the effects of the two reactive nitrogen species from international shipping. Field studies have observed elevated mixing ratios of HONO (0.2 ppb) at a marine site of the Bohai rim in northern China (Wen et al., 2019) and of HONO (126 ppt) and $ClNO_2$ (1.97 ppb) at a coastal site in southern China (Tham et al., 2014, Zha et al., 2014). These observations suggest the significant contribution of ship emissions to the oxidative capacity of the marine and coastal atmosphere in East Asia.

In this study, we used a revised regional chemical transport model to simulate the spatial distributions of HONO and $ClNO_2$ produced by ocean-going ships and their effects on the formation of O_3 and $PM_{2.5}$ in East Asia, which has 8 of the world's top 10 container ports and the world's most trafficked oceans. We selected the summer (July) of 2018 as the study period, when large-scale oceanic winds prevail in Asia; together with the highest radiation and temperature, international shipping is expected to have the most distinctive and perhaps the greatest impact on atmospheric chemistry during the year in East Asia. We describe in Section 2 the details of the model setting, emissions, numerical experiments, observational data, and model

validation. In Section 3, we exhibit the model performance for HONO and $ClNO_2$ and compare the results with available measurements in marine areas; we then show the formation of ship-related HONO and $ClNO_2$ and their subsequent effects on radicals, O_3, and $PM_{2.5}$ in oceanic areas and coastal cities. Our conclusions are given in Section 4.

2. Methodology

2.1 Model Setting

In this study, the WRF–Chem model (version 3.6.1; (Grell et al., 2005) with updated gases-phase and heterogeneous-phase mechanisms of new reactive nitrogen species (Zhang et al., 2017b) was used to simulate the transport, mixing, and chemical transformation of trace gases and aerosols. Briefly, the updated module was based on the default CBMZ module (Zaveri and Peters, 1999), in which the O_3 production came from the traditional photochemical mechanisms with only two gas-phase sources of HONO ($OH+NO \rightarrow HONO$ and $HO_2 + NO_2 \rightarrow HONO$) and no chlorine chemistry. In the updated module (CBMZ-ReNOM), the HONO sources included the additional gas-phase reactions between NO_x and HO_x ($OH+HO_2$), the heterogeneous reaction of NO_2 on the particle, urban, leaf (Kurtenbach et al., 2001), and sea surfaces (Zha et al., 2014), and direct emission from vehicles (Kurtenbach et al., 2001, Gutzwiller et al., 2002, Sun et al., 2020). For this study, an additional HONO source from the photolysis of particulate nitrate ($PNO_3 \rightarrow 0.67HONO + 0.33\ NO_2$) was included into our model. The photolysis rate constant of PNO_3 (J_{PNO3}) was calculated following the approach used in Fu et al. (2019) (namely, $J_{PNO3} = (8.3\times10^{-5}/7\times10^{-7}) \times J_{HNO3\text{-}WRF\text{-}Chem}$, $J_{HNO3-WRF\text{-}Chem}$ is the photolysis rate constant of gaseous HNO_3 calculated online in the WRF-Chem model). For $ClNO_2$ production, the parameterization from Bertram and Thornton (2009) was used to represent the N_2O_5 uptake coefficient and $ClNO_2$ production yield. This parameterization reproduced the order of magnitude and variation of the observed N_2O_5 and $ClNO_2$ levels in a background site of Hong Kong (Dai et al., 2020). The other six chlorine species, with relevant photolysis reactions and subsequent reactions between released Cl radical and VOCs, were also added to the default module (Zhang et al., 2017b). The details of other chemical and physical schemes for the simulation can be found in Zhang et al. (2017b).

The model simulations were performed from June 28 to July 31, 2018. The first 72 h of the simulations were considered as a spin-up time. The initial meteorological conditions were provided by reanalysis data from the final (FNL) Operational Global Analysis dataset provided by the National Centers for Environmental Prediction (NCEP; http://rda.ucar.edu/datasets/ds083.2/). The model had 31 vertical layers with a fixed top of 100 hPa. The domain covered a large part of Asia with a horizontal resolution of 36 × 36 km (Figure 1a). The surface layer was 30 m above the ground, and the lowest 11 layers were approximately within the height of the planetary boundary layer at noon.

2.2 Emissions

Five sets of emission inventories (EIs) were used for anthropogenic emissions in our study. For mainland China, the Multi-resolution Emission Inventory for China (MEIC; http://www.meicmodel.org/) in 2016 was used. For the rest of Asia, we applied the MIX (http://www.meicmodel.org/dataset–mix) for 2010 (Li et al., 2017). For international shipping, the emission database in the Community Emission Data System (CEDS) (McDuffie et al., 2020) for 2017 was used. The HONO emissions from land transportation sources were calculated using their NO_x emissions and the HONO/NO_x ratio of 0.8% for gasoline and 2.3% for diesel. These commonly used ratios in model studies (ref) are based on the previous measurements of vehicle exhausts (Kurtenbach et al., 2001, Gutzwiller et al., 2002) and are generally consistent with more recent emission result (ref). For ship-emitted HONO, we set the emission ratio of HONO/NO_x as 0.51% based on the reported ratio in fresh ship plumes in Chinese waters (Sun et al., 2020). For anthropogenic chloride emissions, the high-resolution (0.1° × 0.1°) EIs of HCl and fine particulate Cl^- for 2014 were applied for mainland China (Fu et al., 2018). These EIs included four sectors and have been shown to offer a reasonable model simulation of particulate chloride by the WRF–Chem model (Dai et al., 2020). The Reactive Chlorine Emission Inventory (RCEI; Keene et al. (1999)) was used for anthropogenic chloride emissions in the other regions. For natural emissions, the biogenic emissions were calculated by the Model of Emission of Gas and Aerosols from Nature (MEGAN) version 2.1 (Guenther et al., 2006).

The spatial distribution of ship NO_x emissions is shown in Figure 1a. The main ship routes with high emission intensity are clearly identified in the ship emission inventory. One major shipping lane is located in the Southern Bay of Bengal (BOB) in the Indian Ocean, passes through the Strait of Malacca, and extends to the South China Sea (SCS) and other Asian countries. Distinct shipping lanes are also shown along the coast of the East China Sea (ECS) and the Sea of Japan (SOJ). Over the West Pacific Ocean (WPO), congested ship routes are distributed among Japan and other countries (Southeast Asian countries, Australia, and North America). Based on the distribution of ship NO_x emissions, six water zones were selected, including three waters around China (SCS, ECS, Bohai Rim (BR)), two waters in other regions (SOJ and BOB), and one open ocean (WPO; Figure 1b). In addition, three densely populated city clusters were chosen (the North Central Plain (NCP), the Yangtze River Delta (YRD), and the Pearl River Delta (PRD)).

2.3 Experimental Setting

Eight simulations were conducted with different emissions and chemistry, as listed in Table 1. In the Def and Def_noship cases, the WRF–Chem model was conducted with default chemistry (i.e., the default CBMZ mechanism with only the two HONO sources and no chlorine chemistry). The differences between Def and Def_noship (i.e., Def-Def_noship) represent the effects of ship emissions with the default nitrogen chemistry. In the Cl and Cl_noship cases, an updated chlorine chemistry in the revised WRF–Chem model was used. The differences between the two cases (i.e., Cl-Cl_noship) represent the effects of ship emissions with the default and additional chlorine chemistry. Similarly, in the HONO and HONO_noship cases, the additional HONO chemistry was used, and the difference between the two cases (i.e., HONO-HONO_noship) represents the default impact of ship emissions with additional HONO chemistry. In the BASE and BASE_noship cases, the integrated HONO and chlorine chemistry are considered. The differences between BASE and BASE_noship represent the shipping impact with the integrated effects of HONO and chlorine species. The results from the BASE experiment will be used to validate the model performance.

2.4 Observational Data and Model Validation

Meteorological data from surface stations from NOAA's National Climatic Data Center (NCDC; Figure S1a) comprising wind direction, wind speed, surface temperature, and specific humidity were used to validate model performance for the meteorological parameters. Conventional air pollutant data (NO_2, $PM_{2.5}$, and O_3) from surface stations (obtained from China's Ministry of Ecology and Environment; Figure S1b) were used to evaluate the simulated air pollutants over China's mainland. Table S2 summarizes the statistical performance of our model results. For meteorological parameters, high R values (>0.85) and low mean bias (MB) indicate good performance for the meteorological field. For regular air pollutants, the model overpredicted $PM_{2.5}$ (MB = 10.6 μg m^{-3}) and slightly underpredicted NO_2 (MB = 3.3 ppbv) and O_3 (MB = 5.5 ppbv). These biases in simulation can be partially explained by uncertainties in the model input, such as the land-use data (Dai et al., 2019) and emission inventory (Li et al., 2017).

The O_3 data from two remote sites (Ryori and Yonagunijima (Yona)) in Japan (https://www.data.jma.go.jp/ghg/kanshi/ghgp/o3) and one coastal background site in Hong Kong (Hok Tsui (HT)) were used to compare the model performance over the maritime areas. These three sites are located along the coasts of the SCS, ECS, and WPO regions (Figure 1b). As shown in Figure S2, with the default chemistry, the model underpredicted the O_3 mixing ratio at the coastal and marine sites, with underestimation by 2.8, 4.8, and 2.3 ppbv at the HT, Ryori, and Yona sites, respectively (Table S3). With the addition of the HONO and $ClNO_2$ chemistry, the simulated O_3 levels at the marine sites were improved, with the MB from –2.8 to –1.5 ppbv at the HT site, –3.0 to –2.3 ppbv at the Ryori site, and –2.3 to –0.7 ppbv at the Yona site.

3 Results

3.1 Simulated HONO and $ClNO_2$ and Contributions from Ship Emissions

Figure 2a shows the horizontal distribution of the average HONO at the surface layer in the BASE case. The predicted HONO was widespread over the oceans, with mixing ratios ranging from 0.005 to 0.300 ppbv and distinct higher concentrations along the main shipping lanes. The distribution of HONO was consistent with that of NO_2 (Figure S3) due to the heterogeneous conversion of NO_2 to form HONO and direct HONO emission from ships. In the vertical

direction, the simulated HONO was concentrated at the surface and reached up to 400 to 600 m in the coastal and marine areas (see Figure S4). Figure 3 shows the vertical profile of HONO from ship emissions in the nine selected regions. Consistent with the overall HONO vertical distribution, ship-contributed HONO also peaked at the surface in the oceanic areas, with average HONO levels of 3 to 120 pptv in the MBL. The greatest contribution of ship emissions was simulated in the WPO (96%), followed by the SOJ (80%), the BOB (49%), three Chinese waters (14% to 16%), and the coastal cities (3% to 12%). The varying ship contributions in these regions can be explained by the relative strength of the emissions from ships and from the adjacent land areas.

High values of $ClNO_2$ were simulated along the coasts and peaked in the lower MBL (Figure 2b), with mixing ratios ranging from 2 to 400 pptv in oceanic areas and the highest value in the BR region. This distribution was in line with that of its precursors N_2O_5 (Figure S5) and particulate chloride (Figure S6). Vertically, the peak value of $ClNO_2$ was simulated in the residual layer (100 to 300 meters; Figure 3), with mixing ratios of 8 to 350 pptv in oceanic areas. Similar to HONO, the greatest ship contribution to $ClNO_2$ was also simulated in the WPO (61%), followed by other oceanic areas (9% to 24%) and coastal cities (5% to 11%).

We compared the modeled HONO and $ClNO_2$ with field observations made at some coastal and marine sites (see Table S4). The simulated HONO mixing ratios were 0.1 to 0.3 ppbv and 0.01 to 0.1 ppbv over BR and SCS, respectively, which were comparable with the measurements at the marine sites of BR (0.2 ppbv) (Wen et al., 2019) and SCS (89 pptv) (Table S4). For the coastal areas of other Asian countries, the simulated HONO compared well with the measurements in South Korea (0.60 ppbv) (Kim et al., 2015) and Japan (0.63 ppbv) (Takeuchi et al., 2013). HONO was simulated at approximately 5 pptv in the open ocean and 10 to 25 pptv along the main shipping lanes (Figure 2a), which were comparable to the measured HONO (3 to 35 pptv) in the open ocean in Europe and North America (Meusel et al., 2016, Kasibhatla et al., 2018, Ye et al., 2016). For $ClNO_2$, the order of magnitude and variation of the measured N_2O_5 and $ClNO_2$ levels at the HT site have been reasonably reproduced by our model for early autumn of 2018 (Dai et al., 2020). The model performance of HONO and $ClNO_2$ in the land areas of mainland China for the summer of 2014 was also evaluated by Zhang et al. (2017). Overall, our model

ability in simulation of HONO and $ClNO_2$ is acceptable, and the model results are sufficiently reliable for further analysis.

3.2 Impact of Ship-Derived HONO and Chlorine on RO_x, O_3, and $PM_{2.5}$

In this section, we evaluate the ship effects on the main atmospheric radicals (RO_x, $OH+HO_2+RO_2$), O_3, and $PM_{2.5}$ with the default chemistry (described in Section 2.3) and with the additional HONO and chlorine chemistry.

3.2.1 RO_x

Figure 4 shows the simulated differences in the average daytime RO_x mixing ratios at the surface from the cases with and without ship emissions using different chemistry. The RO_x mixing ratio was noticeably increased by ship emissions over oceanic areas, and this enhancement was magnified by the additional nitrogen chemistry. With the default chemistry (Figure 4a), the average ship contribution to RO_x was about 18% over the whole oceanic area. The addition of the HONO and chlorine chemistry increased the ship contributions to 28% (Figure 4b) and 22% (Figure 4c), respectively. Photolysis of ship-generated HONO and $ClNO_2$ released radicals (OH and Cl; Figure S7) and recycled NO_x, which then oxidized VOCs and gave rise to high levels of RO_x. With the combined HONO and chlorine chemistry, the ship contribution was further increased to 38% (Figure 4d). This combined ship contribution was smaller than the sum of that from the separate HONO and chlorine chemistry (22% + 28% = 50%), which can be explained by the nonlinear interactions of the chemical system. Figure 5 shows the vertical profile of the RO_x mixing ratio from ship emissions in the nine regions. The enhanced RO_x reached an altitude of greater than 2 km over the oceanic regions, indicating the significant impact of ship-derived HONO and $ClNO_2$ on the oxidative capacity in the marine troposphere.

The largest increase in the ship contribution to RO_x was predicted in the WPO region (from 29% to 50%; Figure 9a), followed by other oceanic areas (from 3% to 12% to 6% to 17%) and coastal cities (from –2% to 3% to 4% to 6%). The maximum ship contribution in the WPO region was consistent with the greatest ship contribution to HONO and $ClNO_2$ in this region (Figure 4d). In

the SCS and BOB regions, the enhanced RO_x was more dispersed with the combined nitrogen chemistry than that with the default and separate nitrogen chemistry. In the coastal cities, the RO_x mixing ratio was also affected by ship emissions via the transport of ship-generated HONO and $ClNO_2$ by summertime winds.

3.2.2 O_3

Figure 6 shows the simulated differences in the average O_3 at the surface from the cases with and without ship emissions. Consistent with the impact of ship emissions on oceanic RO_x, the oceanic O_3 was also noticeably increased (by 9%) by ship emissions, which was further enhanced by the addition of HONO (12%) and $ClNO_2$ (14%) and combined nitrogen chemistry (21%). The simulated distribution of ship-enhanced O_3 with the default chemistry was along the main shipping routes with high NO_x emissions (Figure 6a). O_3 formation was highly sensitive to NO_x from ship emissions due to the relatively low concentrations of NO_x in the marine areas. The larger ship contribution with $ClNO_2$ chemistry than with HONO chemistry may be partially explained by a higher production ozone efficiency by NO_2 than by NO (from photolysis of HONO) and by the faster reaction rate of Cl radicals than OH radicals with long-lived alkanes.

With the combined impact from HONO and $ClNO_2$, widespread ozone increases were simulated over the SCS, BOB, and WPO regions (Figure 6d). The combined nitrogen chemistry also increased the ozone concentrations in the coastal areas; in contrast, these concentrations were decreased by HONO or $ClNO_2$ separately. As shown in Figure 6b and c, distinct ozone enhancement was simulated over the marine area of South Korea and Japan by HONO or $ClNO_2$. However, this enhancement was weakened and even canceled by their combined effects. We calculated an indicator of the ozone formation regimes based on the ratio of the production rate of H_2O_2 to that of HNO_3 (P_{H2O2}/P_{HNO3}) (Fu et al., 2020). Figure 7, with the combined HONO and $ClNO_2$ chemistry, shows that the NO_x-sensitive regime in east Asia was changed to a VOC-sensitive regime, which was probably due to the increase level of NO or NO_2 from photolysis of HONO.

Figure S8 shows the vertical profile of ship-generated O_3 enhancement in the nine regions. Similar to ship-enhanced RO_x, ship-related O_3 enhancement stretched from the surface to the lower troposphere (>2 km) over the marine regions. Because the emissions from ships occur at the sea surface, the vertically enhanced O_3 formation was caused by strong convection (Dalsøren et al., 2009)

The ship contribution to O_3 formation was also simulated in the WPO region (from 21% to 38%; Figure 9b). In other oceanic areas, the contributions of ship emissions were also increased from 3% to 18% to 12% to 24%, with two distinct O_3 enhancements over the BR (~10 ppbv; Figure 6d) and ECS (15 ppbv) regions. In the three coastal city clusters, the reduced O_3 formation was simulated by ship emissions with the default chemistry (from –5 to –1 ppb). Because these coastal cities are in the VOC-limited regime (Figure 7a), the NO_x from ships would lead to a decrease in chemical O_3 production. With the combined HONO and $ClNO_2$ effects, the ship-induced O_3 increased to –1 to –5 ppb due to the enhanced radicals and the transport of O_3 in the marine areas by ship-generated HONO and $ClNO_2$. The maximum O_3 increase in coastal cities also doubled from 3 ppb (5%) to 7 ppb (11%), aggravating the negative effects of ship emissions on human health in coastal cities.

In addition to the above coastal and oceanic areas, ship emissions also exert considerable impact on surface O_3 in distant inland areas such as Sichuan basin, and interestingly there are some 'hot spots' of ozone increase/decrease in the inland areas due to ship emissions (Figure 6a-d) (as well as ROx (Figure 4a-d) and $PM_{2.5}$ (Figure 8a-d)). These hot spots may be a result of inhomogeneous impact of ship emissions due to complicated dynamic and chemical processes that affect the fate and distribution of ship-emitted pollutants in the inland areas. In particular, the mountainous terrains in south China may have large influence on transport of ship emissions to the inland areas.

3.2.3 $PM_{2.5}$

Ship-derived HONO and $ClNO_2$ also influence the production of aerosols via changes in radicals and NO_x. Figure 8 shows the simulated differences in the average $PM_{2.5}$ at the surface for cases with and without ship emissions. The $PM_{2.5}$ concentration was considerately enhanced by ship

emissions, and the additional nitrogen chemistry further increased the simulated $PM_{2.5}$ concentration. With the default chemistry, the average ship contribution to the $PM_{2.5}$ concentration was about 7% in oceanic areas (Figure 8a), and it was increased to 10% with the addition of HONO and $ClNO_2$ chemistry (Figure 8d). The greatest contribution from shipping to the $PM_{2.5}$ concentration was also simulated over the WPO region, as with ozone, with the contribution ranging from 13% with the default chemistry to 19% with the improved chemistry (Figure 9c). In other oceanic areas, the ship contributions were also increased from 2% to 12% to 6% to 15%. We calculated the effects of ship-generated HONO and $ClNO_2$ on the formation of secondary particles. The additional ship HONO and chlorine chemistry increased the ship contribution to particulate nitrate from 13% to 41% in oceanic areas (Figure S9 and Figure S11) and its contribution to particulate sulfate from 11% to 34% (Figure S10 and Figure S11). In the coastal cities, the default contribution by ships was about 4% to 8%, which was also increased to 4% to 12% with the improved chemistry (Figure 9c). The considerable increase in ship-contributed $PM_{2.5}$ and ozone due to HONO and $ClNO_2$ demonstrates the need to consider these compounds in evaluations of the impact of shipping on air quality.

Previous studies have evaluated the impact of ship emissions on the formation of O_3 and $PM_{2.5}$. Aksoyoglu et al. (2016) simulated the average ship contribution to oceanic O_3 as 10% to 20% in the Mediterranean area, and Huszar et al. (2010) showed a ship contribution of 10% over the Eastern Atlantic. The maximum O_3 enhancement by ship emissions was 15 ppb in the coastal waters of South Korea (Song et al., 2010) and 30 to 50 $\mu g\ m^{-3}$ off the coast of the YRD region (Wang et al., 2019). For $PM_{2.5}$, the average ship contributions were about 20% to 25% in European waters (Aksoyoglu et al., 2016) and 2.2% to 18.8% off the coast of China (Lv et al., 2018).

Compared to previous studies, our study simulated a higher contribution to average ozone formation and a smaller contribution to average $PM_{2.5}$. We note that the underprediction of NO_2 in our simulation may lead to an underestimation of HONO, and the over predicted $PM_{2.5}$ can result in the overestimation of N_2O_5 uptake, conversion of NO_2 to HONO, and production of $ClNO_2$. The exact effects of these uncertainties on the ozone and $PM_{2.5}$ is difficult to quantify. It is also difficult to discern the differences in our and previous modeling studies due to the differences in the methodologies adopted, including ship emission inventory, model resolution,

chemical mechanisms (in addition to different treatment of HONO and $ClNO_2$ chemistry), and period of study. However, all these studies demonstrate an important impact of ship emissions on atmospheric chemistry and air quality. The key finding of our study is the role of HONO and $ClNO_2$ in driving the oxidation processes, which has not been fully considered in most previous model studies of the impact of shipping on pollutant levels.

4 Conclusions

This study evaluated the production of HONO and $ClNO_2$ from international shipping and their impact on the oxidative capacity, ozone level, and level of fine PM in the maritime and coastal areas of eastern Asia. The results show that photolysis of the two compounds releases OH and Cl radicals, recycles NO_x, and changes conventional hydroxyl and organic peroxy radicals (RO_x = OH + HO_2 + RO_2) by 0.8% to 21.4% (0.8-7.7% over coasts and 2.6-21.4% over oceans), O_3 by 5.9% to 16.6% (6.9-14.6% over coasts and 5.9-16.6% over oceans) and $PM_{2.5}$ by -1.2% to 8.6% (-1.2-6% over coasts and 3.2-8.6% over oceans) at the surface of the western Pacific regions. Their impact extends to the marine boundary layer. The largest contributions of HONO and $ClNO_2$ occur in the relatively remote oceans. Because ocean-going ships are a major source of NO_x, which is the key chemical precursor to HONO and $ClNO_2$, it is important to consider the sources and chemistry of these nitrogen compounds in evaluations of the impact of ship emissions.

Code and data availability. The codes and data used in this study are available upon request from Tao Wang (cetwang@polyu.edu.hk).

Author contributions. TW initiated the research, and JD and TW designed the paper framework. JD ran the model, processed the data, and made the plots. JD and TW analyzed the results and wrote the paper.

Acknowledgments. We would like to thank Qiang Zhang from Tsinghua University for providing the emission inventory and Xiao Fu from The Hong Kong Polytechnic University for providing the code of HONO sources and anthropogenic chloride emission inventory.

Financial support. This research has been supported by the Hong Kong Research Grants Council (grant no. T24-504/17-N) and the National Natural Science Foundation of China (grant no. 91844301).

References

AKSOYOGLU, S., BALTENSPERGER, U. & PRÉVÔT, A. S. 2016. Contribution of ship emissions to the concentration and deposition of air pollutants in Europe. *Atmospheric Chemistry & Physics,* 16.

ANDERSSON, C., BERGSTRÖM, R. & JOHANSSON, C. 2009. Population exposure and mortality due to regional background PM in Europe–Long-term simulations of source region and shipping contributions. *Atmospheric Environment,* 43**,** 3614-3620.

BERTRAM, T. & THORNTON, J. 2009. Toward a general parameterization of N2O5 reactivity on aqueous particles: the competing effects of particle liquid water, nitrate and chloride. *Atmos. Chem. Phys,* 9**,** 8351-8363.

CAMPLING, P., JANSSEN, L., VANHERLE, K., COFALA, J., HEYES, C. & SANDER, R. 2013. Specific evaluation of emissions from shipping including assessment for the establishment of possible new emission control areas in European Seas. *Flemish Institute for Technological Research (VITO), Mol, BE*.

CORBETT, J. J. & FISCHBECK, P. 1997. Emissions from ships. *Science,* 278**,** 823-824.

CORBETT, J. J., WINEBRAKE, J. J., GREEN, E. H., KASIBHATLA, P., EYRING, V. & LAUER, A. 2007. Mortality from ship emissions: a global assessment. *Environmental science & technology,* 41**,** 8512-8518.

DAI, J., LIU, Y., WANG, P., FU, X., XIA, M. & WANG, T. 2020. The impact of sea-salt chloride on ozone through heterogeneous reaction with N2O5 in a coastal region of south China. *Atmospheric Environment***,** 117604.

DAI, J., WANG, X., DAI, W. & CHANG, M. 2019. The impact of inhomogeneous urban canopy parameters on meteorological conditions and implication for air quality in the Pearl River Delta region. *Urban Climate,* 29**,** 100494.

DEVASTHALE, A., KRÜGER, O. & GRAßL, H. 2006. Impact of ship emissions on cloud properties over coastal areas. *Geophysical research letters,* 33.

EYRING, V., ISAKSEN, I. S., BERNTSEN, T., COLLINS, W. J., CORBETT, J. J., ENDRESEN, O., GRAINGER, R. G., MOLDANOVA, J., SCHLAGER, H. & STEVENSON, D. S. 2010. Transport impacts on atmosphere and climate: Shipping. *Atmospheric Environment,* 44**,** 4735-4771.

EYRING, V., KÖHLER, H., VAN AARDENNE, J. & LAUER, A. 2005. Emissions from international shipping: 1. The last 50 years. *Journal of Geophysical Research: Atmospheres,* 110.

FINLAYSON-PITTS, B., WINGEN, L., SUMNER, A., SYOMIN, D. & RAMAZAN, K. 2003. The heterogeneous hydrolysis of NO 2 in laboratory systems and in outdoor and indoor atmospheres: An integrated mechanism. *Physical Chemistry Chemical Physics,* 5**,** 223-242.

FU, X., WANG, T., GAO, J., WANG, P., LIU, Y., WANG, S., ZHAO, B. & XUE, L. 2020. Persistent Heavy Winter Nitrate Pollution Driven by Increased Photochemical Oxidants in Northern China. *Environmental Science & Technology,* 54**,** 3881-3889.

FU, X., WANG, T., WANG, S., ZHANG, L., CAI, S., XING, J. & HAO, J. 2018. Anthropogenic emissions of hydrogen chloride and fine particulate chloride in China. *Environmental science & technology,* 52**,** 1644-1654.

FU, X., WANG, T., ZHANG, L., LI, Q., WANG, Z., XIA, M., YUN, H., WANG, W., YU, C. & YUE, D. 2019. The significant contribution of HONO to secondary pollutants during a severe winter pollution event in southern China.

FUGLESTVEDT, J., BERNTSEN, T., EYRING, V., ISAKSEN, I., LEE, D. S. & SAUSEN, R. 2009. Shipping Emissions: From Cooling to Warming of Climate・ and Reducing Impacts on Health. ACS Publications.

GRELL, G. A., PECKHAM, S. E., SCHMITZ, R., MCKEEN, S. A., FROST, G., SKAMAROCK, W. C. & EDER, B. 2005. Fully coupled "online" chemistry within the WRF model. *Atmospheric Environment,* 39**,** 6957-6975.

GUENTHER, A., KARL, T., HARLEY, P., WIEDINMYER, C., PALMER, P. & GERON, C. 2006. Estimates of global terrestrial isoprene emissions using MEGAN (Model of Emissions of Gases and Aerosols from Nature).

GUTZWILLER, L., ARENS, F., BALTENSPERGER, U., GÄGGELER, H. W. & AMMANN, M. 2002. Significance of semivolatile diesel exhaust organics for secondary HONO formation. *Environmental science & technology,* 36**,** 677-682.

HOOR, P., BORKEN-KLEEFELD, J., CARO, D., DESSENS, O., ENDRESEN, O., GAUSS, M., GREWE, V., HAUGLUSTAINE, D., ISAKSEN, I. S. & JÖCKEL, P. 2009. The impact of traffic emissions on atmospheric ozone and OH: results from QUANTIFY. *Atmospheric Chemistry and Physics,* 9**,** 3113-3136.

HUSZAR, P., CARIOLLE, D., PAOLI, R., HALENKA, T., BELDA, M., SCHLAGER, H., MIKSOVSKY, J. & PISOFT, P. 2010. Modeling the regional impact of ship emissions on NOx and ozone levels over the Eastern Atlantic and Western Europe using ship plume parameterization. *Atmospheric Chemistry and Physics,* 10**,** 6645-6660.

KASIBHATLA, P., SHERWEN, T., EVANS, M. J., CARPENTER, L. J., REED, C., ALEXANDER, B., CHEN, Q., SULPRIZIO, M. P., LEE, J. D. & READ, K. A. 2018. Global impact of nitrate photolysis in sea-salt aerosol on NOx, OH, and O3 in the marine boundary layer. *Atmospheric Chemistry and Physics***,** 11185-11203.

KEENE, W. C., KHALIL, M. A. K., ERICKSON III, D. J., MCCULLOCH, A., GRAEDEL, T. E., LOBERT, J. M., AUCOTT, M. L., GONG, S. L., HARPER, D. B. & KLEIMAN, G. 1999. Composite global emissions of reactive chlorine from anthropogenic and natural sources: Reactive Chlorine Emissions Inventory. *Journal of Geophysical Research: Atmospheres,* 104**,** 8429-8440.

KIM, S., KIM, S.-Y., LEE, M., SHIM, H., WOLFE, G., GUENTHER, A. B., HE, A., HONG, Y. & HAN, J. 2015. Impact of isoprene and HONO chemistry on ozone and OVOC formation in a semirural South Korean forest. *Atmospheric Chemistry and Physics (Online),* 15.

KLEFFMANN, J., GAVRILOAIEI, T., HOFZUMAHAUS, A., HOLLAND, F., KOPPMANN, R., RUPP, L., SCHLOSSER, E., SIESE, M. & WAHNER, A. 2005. Daytime formation of nitrous acid: A major source of OH radicals in a forest. *Geophysical Research Letters,* 32.

KURTENBACH, R., BECKER, K., GOMES, J., KLEFFMANN, J., LÖRZER, J., SPITTLER, M., WIESEN, P., ACKERMANN, R., GEYER, A. & PLATT, U. 2001. Investigations of emissions and heterogeneous formation of HONO in a road traffic tunnel. *Atmospheric Environment,* 35**,** 3385-3394.

LAWRENCE, M. G. & CRUTZEN, P. J. 1999. Influence of NO x emissions from ships on tropospheric photochemistry and climate. *Nature,* 402**,** 167-170.

LI, M., ZHANG, Q., KUROKAWA, J.-I., WOO, J.-H., HE, K., LU, Z., OHARA, T., SONG, Y., STREETS, D. G. & CARMICHAEL, G. R. 2017. MIX: a mosaic Asian anthropogenic emission inventory under the international collaboration framework of the MICS-Asia and HTAP. *Atmospheric Chemistry and Physics (Online),* 17.

LI, Q., ZHANG, L., WANG, T., THAM, Y. J., AHMADOV, R., XUE, L., ZHANG, Q. & ZHENG, J. 2016. Impacts of heterogeneous uptake of dinitrogen pentoxide and chlorine activation on ozone and reactive nitrogen partitioning: improvement and application of the WRF-Chem model in southern China. *Atmospheric chemistry and physics*.

LIU, H., FU, M., JIN, X., SHANG, Y., SHINDELL, D., FALUVEGI, G., SHINDELL, C. & HE, K. 2016. Health and climate impacts of ocean-going vessels in East Asia. *Nature climate change,* 6**,** 1037-1041.

LIU, H., JIN, X., WU, L., WANG, X., FU, M., LV, Z., MORAWSKA, L., HUANG, F. & HE, K. 2018. The impact of marine shipping and its DECA control on air quality in the Pearl River Delta, China. *Science of The Total Environment,* 625**,** 1476-1485.

LV, Z., LIU, H., YING, Q., FU, M., MENG, Z., WANG, Y., WEI, W., GONG, H. & HE, K. 2018. Impacts of shipping emissions on PM2: 5 pollution in China. *Atmospheric Chemistry & Physics,* 18.

MCDUFFIE, E. E., SMITH, S. J., O'ROURKE, P., TIBREWAL, K., VENKATARAMAN, C., MARAIS, E. A., ZHENG, B., CRIPPA, M., BRAUER, M. & MARTIN, R. V. 2020. A global anthropogenic emission inventory of atmospheric pollutants from sector-and fuel-specific sources (1970–2017): An application of the Community Emissions Data System (CEDS). *Earth System Science Data Discussions***,** 1-49.

MEUSEL, H., KUHN, U., REIFFS, A., MALLIK, C., HARDER, H., MARTINEZ, M., SCHULADEN, J., BOHN, B., PARCHATKA, U. & CROWLEY, J. N. 2016. Daytime formation of nitrous acid at a coastal remote site in Cyprus indicating a common ground source of atmospheric HONO and NO. *Atmospheric Chemistry and Physics,* 16**,** 14475-14493.

MOLDANOVÁ, J., FRIDELL, E., POPOVICHEVA, O., DEMIRDJIAN, B., TISHKOVA, V., FACCINETTO, A. & FOCSA, C. 2009. Characterisation of particulate matter and gaseous emissions from a large ship diesel engine. *Atmospheric Environment,* 43**,** 2632-2641.

MONGE, M. E., D'ANNA, B., MAZRI, L., GIROIR-FENDLER, A., AMMANN, M., DONALDSON, D. & GEORGE, C. 2010. Light changes the atmospheric reactivity of soot. *Proceedings of the National Academy of Sciences,* 107**,** 6605-6609.

NDOUR, M., D'ANNA, B., GEORGE, C., KA, O., BALKANSKI, Y., KLEFFMANN, J., STEMMLER, K. & AMMANN, M. 2008. Photoenhanced uptake of NO2 on mineral dust: Laboratory experiments and model simulations. *Geophysical Research Letters,* 35.

OSTHOFF, H. D., ROBERTS, J. M., RAVISHANKARA, A., WILLIAMS, E. J., LERNER, B. M., SOMMARIVA, R., BATES, T. S., COFFMAN, D., QUINN, P. K. & DIBB, J. E. 2008. High levels of nitryl chloride in the polluted subtropical marine boundary layer. *Nature Geoscience,* 1**,** 324.

SARWAR, G., SIMON, H., XING, J. & MATHUR, R. 2014. Importance of tropospheric ClNO2 chemistry across the Northern Hemisphere. *Geophysical Research Letters,* 41**,** 4050-4058.

SIMON, H., KIMURA, Y., MCGAUGHEY, G., ALLEN, D., BROWN, S., OSTHOFF, H., ROBERTS, J., BYUN, D. & LEE, D. 2009. Modeling the impact of ClNO2 on ozone formation in the Houston area. *Journal of Geophysical Research: Atmospheres,* 114.

SONG, S.-K., SHON, Z.-H., KIM, Y.-K., KANG, Y.-H., OH, I.-B. & JUNG, C.-H. 2010. Influence of ship emissions on ozone concentrations around coastal areas during summer season. *Atmospheric Environment,* 44**,** 713-723.

SUN, L., CHEN, T., JIANG, Y., ZHOU, Y., SHENG, L., LIN, J., LI, J., DONG, C., WANG, C. & WANG, X. 2020. Ship emission of nitrous acid (HONO) and its impacts on the marine atmospheric oxidation chemistry. *Science of The Total Environment***,** 139355.

TAKEUCHI, M., MIYAZAKI, Y., TSUNODA, H. & TANAKA, H. 2013. Atmospheric acid gases in Tokushima, Japan, monitored with parallel plate wet denuder coupled ion chromatograph. *Analytical Sciences,* 29**,** 165-168.

THAM, Y. J., YAN, C., XUE, L., ZHA, Q., WANG, X. & WANG, T. 2014. Presence of high nitryl chloride in Asian coastal environment and its impact on atmospheric photochemistry. *Chinese science bulletin,* 59**,** 356-359.

UNCTAD 2019. Review of Maritime Transport. *UNITED NATIONS PUBLICATION***,** 28.

WANG, R., TIE, X., LI, G., ZHAO, S., LONG, X., JOHANSSON, L. & AN, Z. 2019. Effect of ship emissions on O3 in the Yangtze River Delta region of China: Analysis of WRF-Chem modeling. *Science of The Total Environment,* 683**,** 360-370.

WANG, T., THAM, Y. J., XUE, L., LI, Q., ZHA, Q., WANG, Z., POON, S. C., DUBÉ, W. P., BLAKE, D. R. & LOUIE, P. K. 2016. Observations of nitryl chloride and modeling its source and effect on ozone in the planetary boundary layer of southern China. *Journal of Geophysical Research: Atmospheres,* 121**,** 2476-2489.

WEN, L., CHEN, T., ZHENG, P., WU, L., WANG, X., MELLOUKI, A., XUE, L. & WANG, W. 2019. Nitrous acid in marine boundary layer over eastern Bohai Sea, China: Characteristics, sources, and implications. *Science of the total environment,* 670**,** 282-291.

YE, C., ZHANG, N., GAO, H. & ZHOU, X. 2017. Photolysis of Particulate Nitrate as a Source of HONO and NO x. *Environmental Science & Technology,* 51**,** 6849-6856.

YE, C., ZHOU, X., PU, D., STUTZ, J., FESTA, J., SPOLAOR, M., TSAI, C., CANTRELL, C., MAULDIN, R. L. & CAMPOS, T. 2016. Rapid cycling of reactive nitrogen in the marine boundary layer. *Nature,* 532**,** 489-491.

ZAVERI, R. A. & PETERS, L. K. 1999. A new lumped structure photochemical mechanism for large‐scale applications. *Journal of Geophysical Research: Atmospheres,* 104**,** 30387-30415.

ZHA, Q., XUE, L., WANG, T., XU, Z., YEUNG, C., LOUIE, P. K. & LUK, C. W. 2014. Large conversion rates of NO2 to HNO2 observed in air masses from the South China Sea: Evidence of strong production at sea surface? *Geophysical Research Letters,* 41**,** 7710-7715.

ZHANG, L., LI, Q., WANG, T., AHMADOV, R., ZHANG, Q., LI, M. & LV, M. 2017a. Combined impacts of nitrous acid and nitryl chloride on lower-tropospheric ozone: new module development in WRF-Chem and application to China. *Atmospheric chemistry physics***,** 9733-9750.

ZHANG, L., LI, Q., WANG, T., AHMADOV, R., ZHANG, Q., LI, M. & LV, M. 2017b. Combined impacts of nitrous acid and nitryl chloride on lower-tropospheric ozone: new module development in WRF-Chem and application to China.

ZHANG, Y., WEN, X. Y., WANG, K., VIJAYARAGHAVAN, K. & JACOBSON, M. Z. 2009. Probing into regional O3 and particulate matter pollution in the United States: 2. An examination of formation mechanisms through a process analysis technique and sensitivity study. *Journal of Geophysical Research: Atmospheres,* 114.

ZHANG, Y., YANG, X., BROWN, R., YANG, L., MORAWSKA, L., RISTOVSKI, Z., FU, Q. & HUANG, C. 2017c. Shipping emissions and their impacts on air quality in China. *Science of the Total Environment,* 581**,** 186-198.

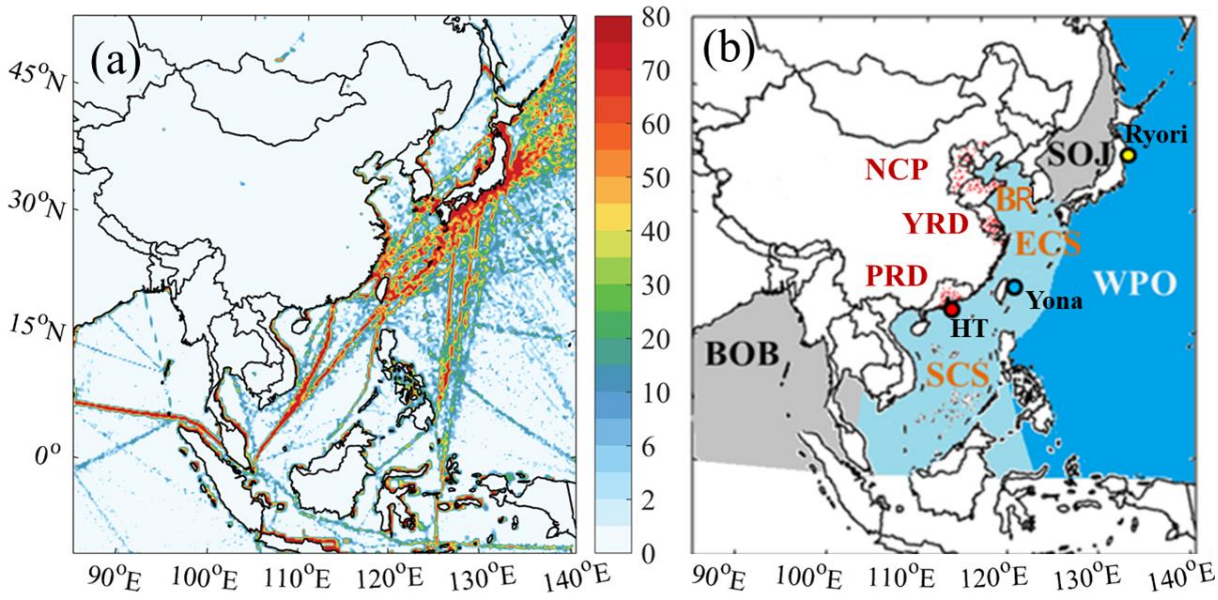

Figure 1: (a) NO_x emission fluxes from ships (Unit: g m^{-2} $month^{-1}$) in July 2017. (b) Model domains with six water zones (South China Sea (SCS), East China Sea (ECS), Bohai rim (BR), Sea of Japan (SOJ), Bay of Bengal (BOB), and West Pacific Ocean (WPO)), three coastal city clusters (Pearl River Delta (PRD), Yangtze River Delta (YRD) and North Central Plain (NCP)), and three maritime observational sites (Hok Tsui (HT), Yonagunijima (Yona), and Ryori). Red dots in PRD, YRD, and NCP represent selected coastal sites. Ranges of latitude and longitude in each body of water are listed in Table S1 in the supplementary information.

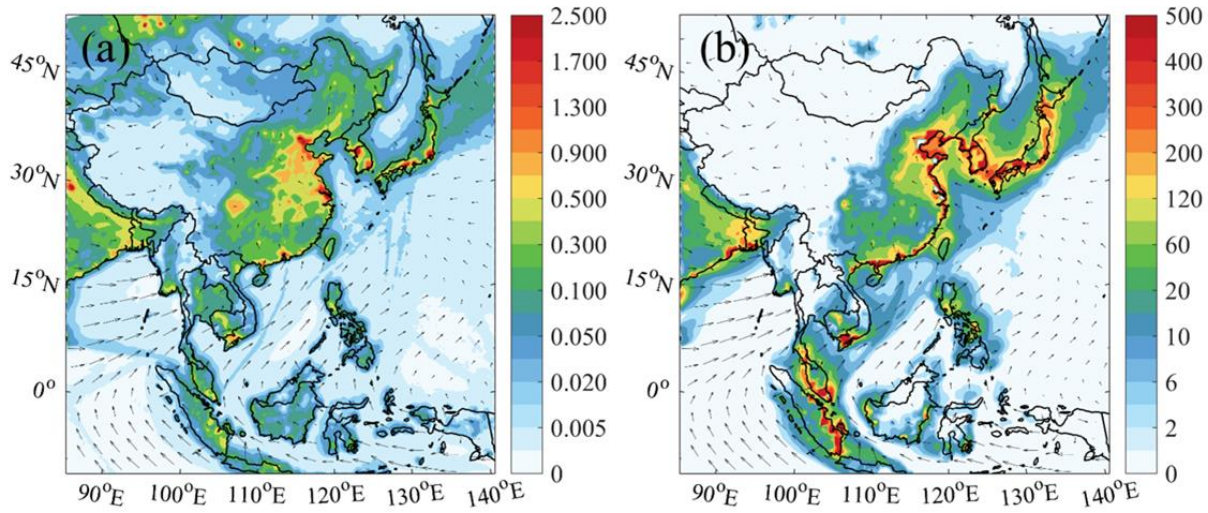

Figure 2: Spatial distributions of the simulation of averaged (a) HONO (Unit: ppbv, whole day) and (b) nighttime $ClNO_2$ (Unit: pptv, 18:00 – 06:00 Local Standard Time (LST)) at the surface layer (~30 m) in July 2018 from the BASE case. Arrows present simulated wind vectors from the BASE case.

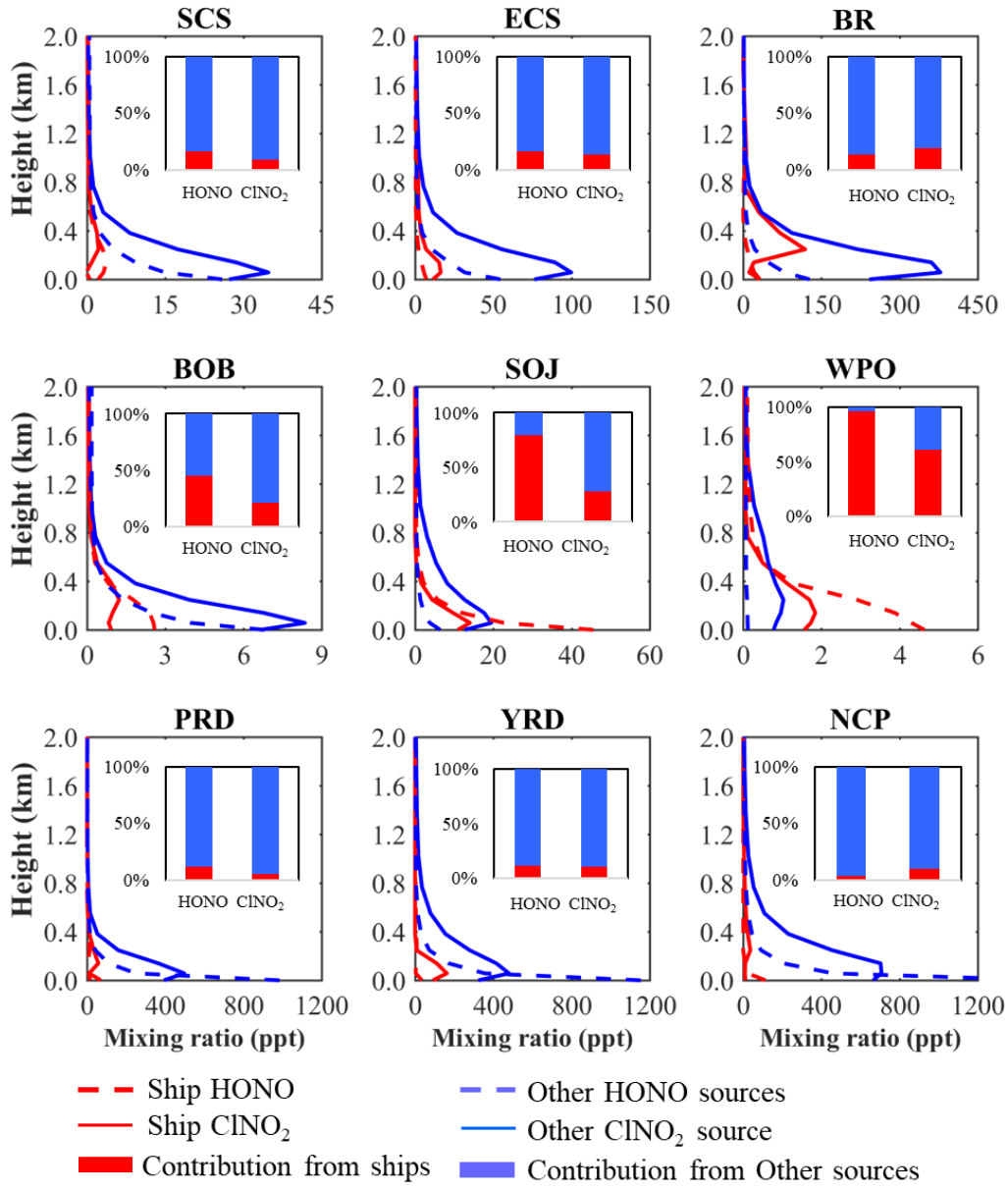

600

Figure 3: Vertical profiles of simulated HONO and nighttime $ClNO_2$ (Unit: ppt) from ship emissions and other sources in nine regions. Also shown are contributions of ship emissions and other sources to averaged HONO and nighttime $ClNO_2$ levels in the marine boundary layer (within 600 m).

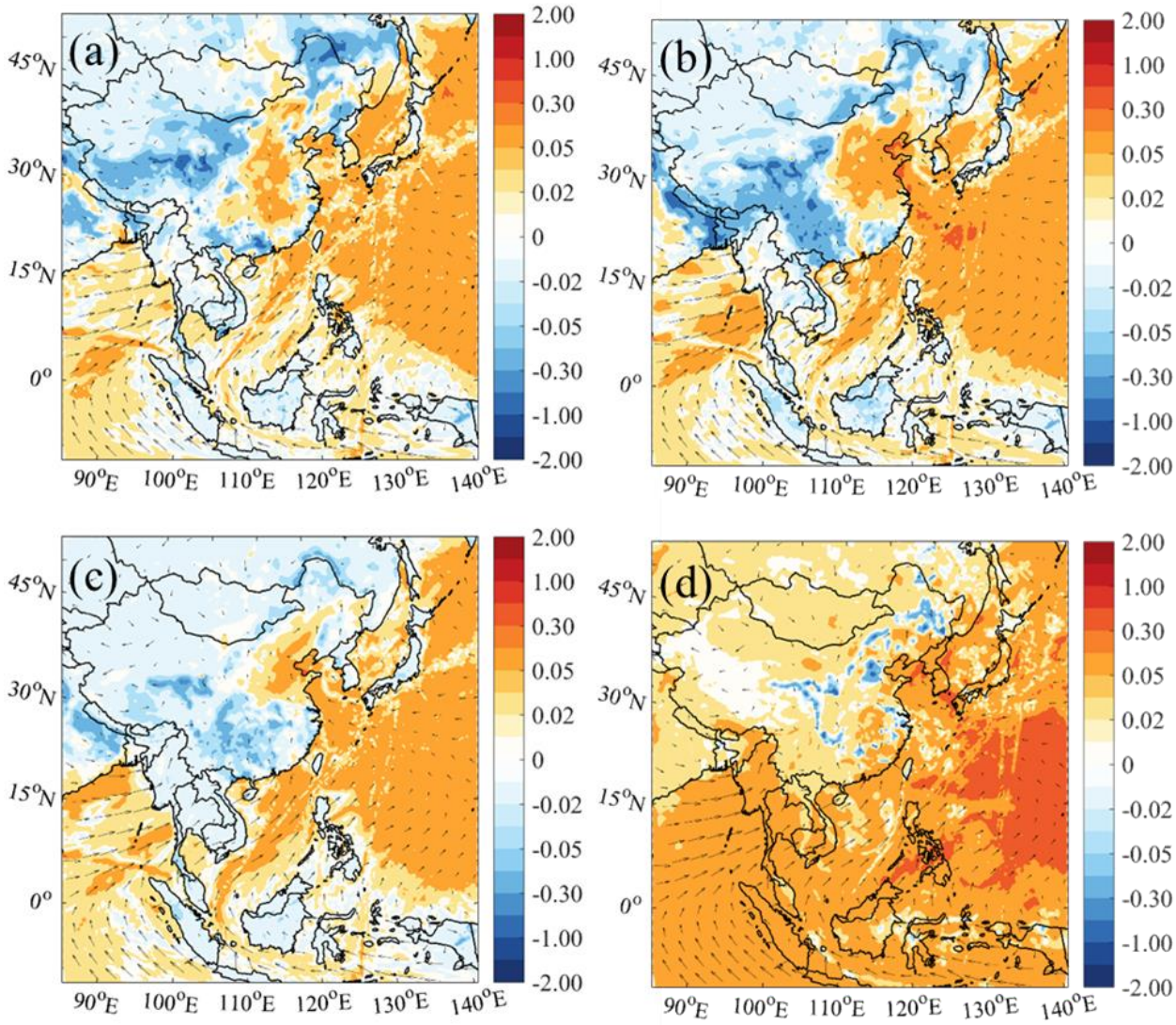

605

Figure 4: Averaged daytime RO_x changes due to ship emisisons (06:00-18:00 LST; Unit: pptv) with (a) default chemistry (Def-Def_noship), (b) default and additional HONO chemistry (HONO-HONO_noship), (c) default and additional chlorine chemistry (Cl-Cl_noship), and (d) default and combined HONO and chlorine chemistry (BASE-BASE_noship). Arrows present simulated wind vectors from BASE case.

610

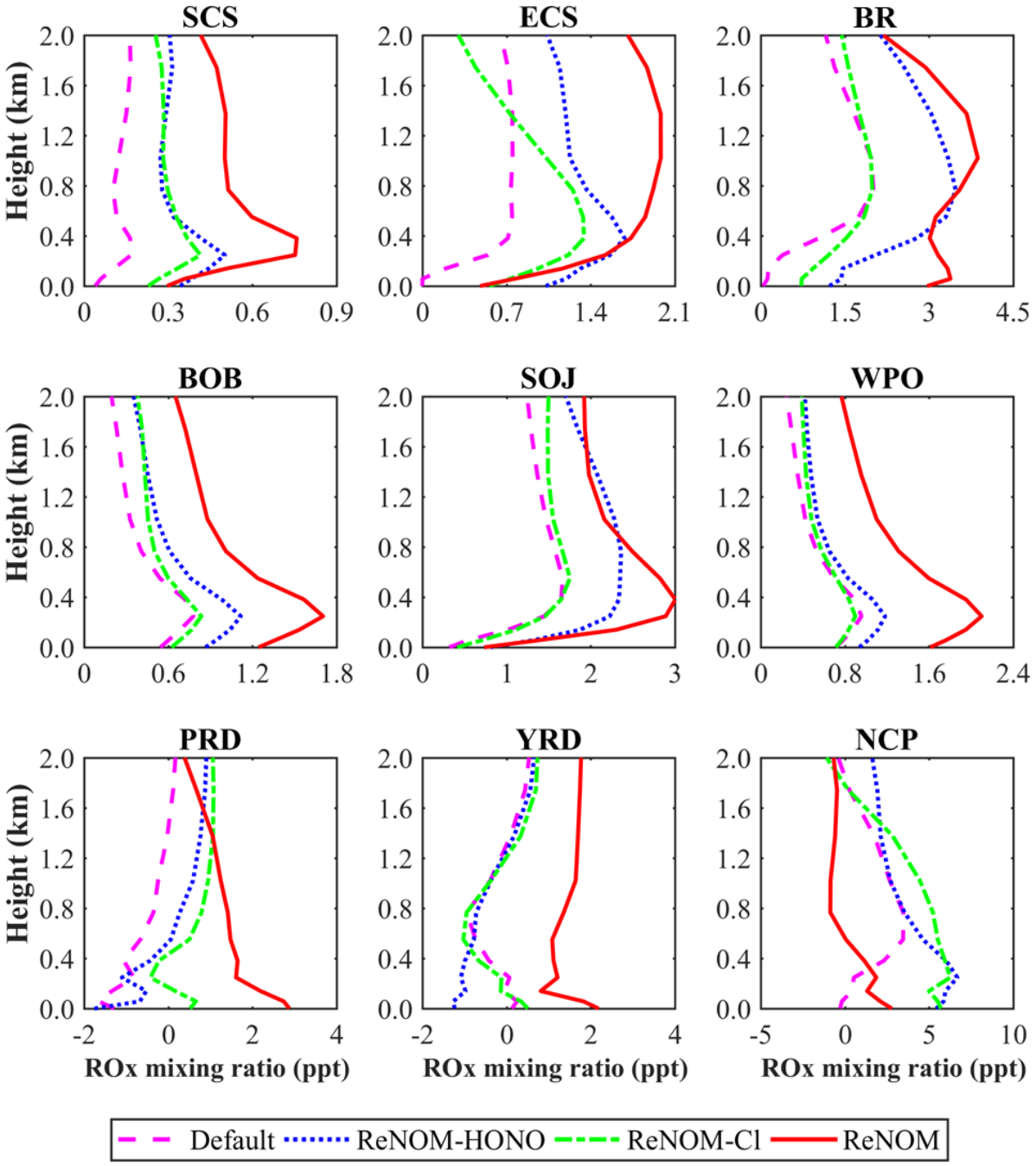

615

Figure 5: Vertical profiles of daytime RO_x changes due to ship emissions (Unit: pptv) from different chemistry in nine regions.

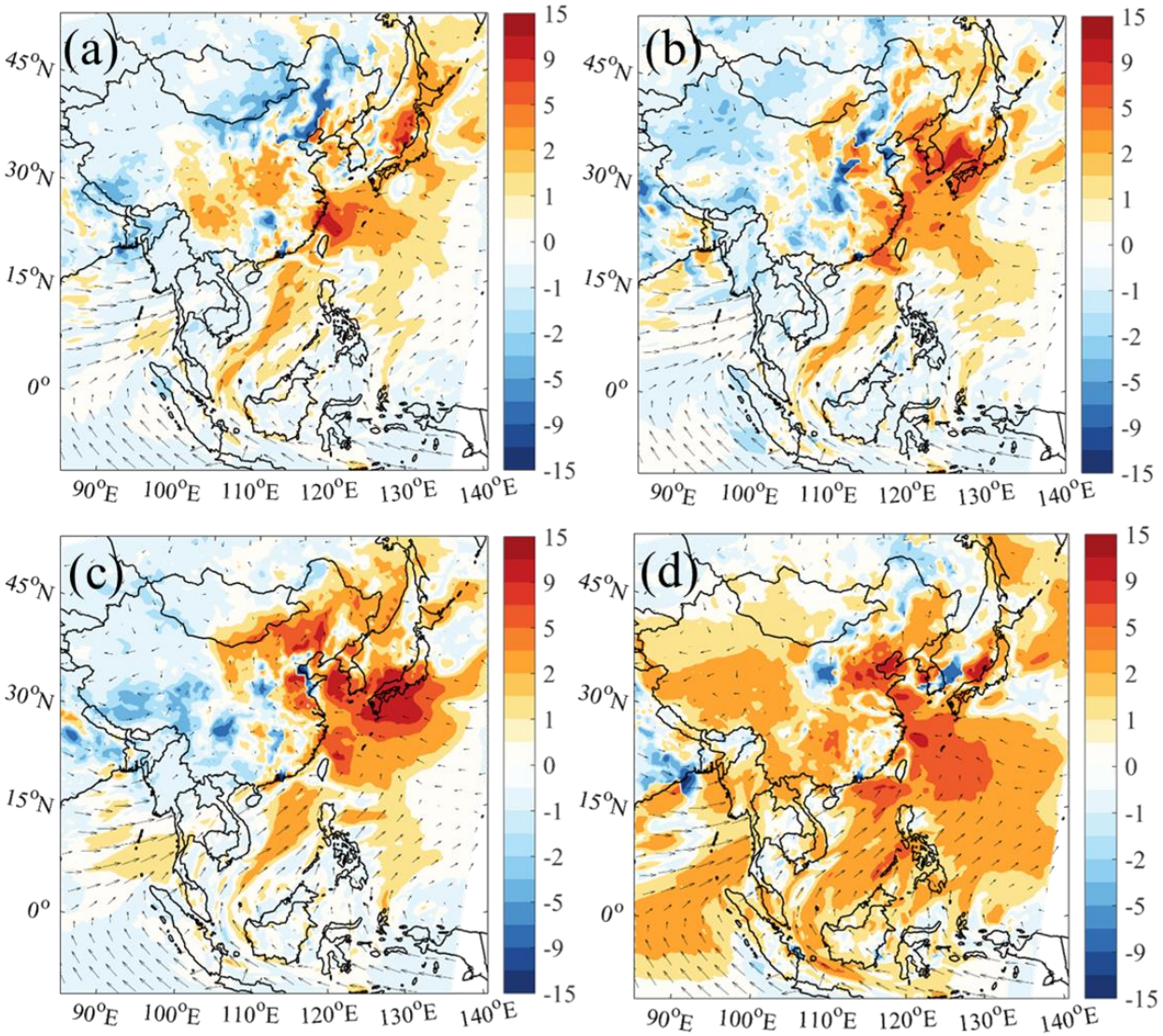

620

Figure 6: 24-hour averaged ozone changes (06:00-18:00 LST; Unit: ppbv) due to ship emissions with (a) default chemistry (Def-Def_noship), (b) default and additional HONO chemistry (HONO-HONO_noship), (c) default and additional chlorine chemistry (Cl-Cl_noship), and (d) default and combined HONO and chlorine chemistry (BASE-
625 **BASE_noship). Arrows present simulated wind vectors from BASE case.**

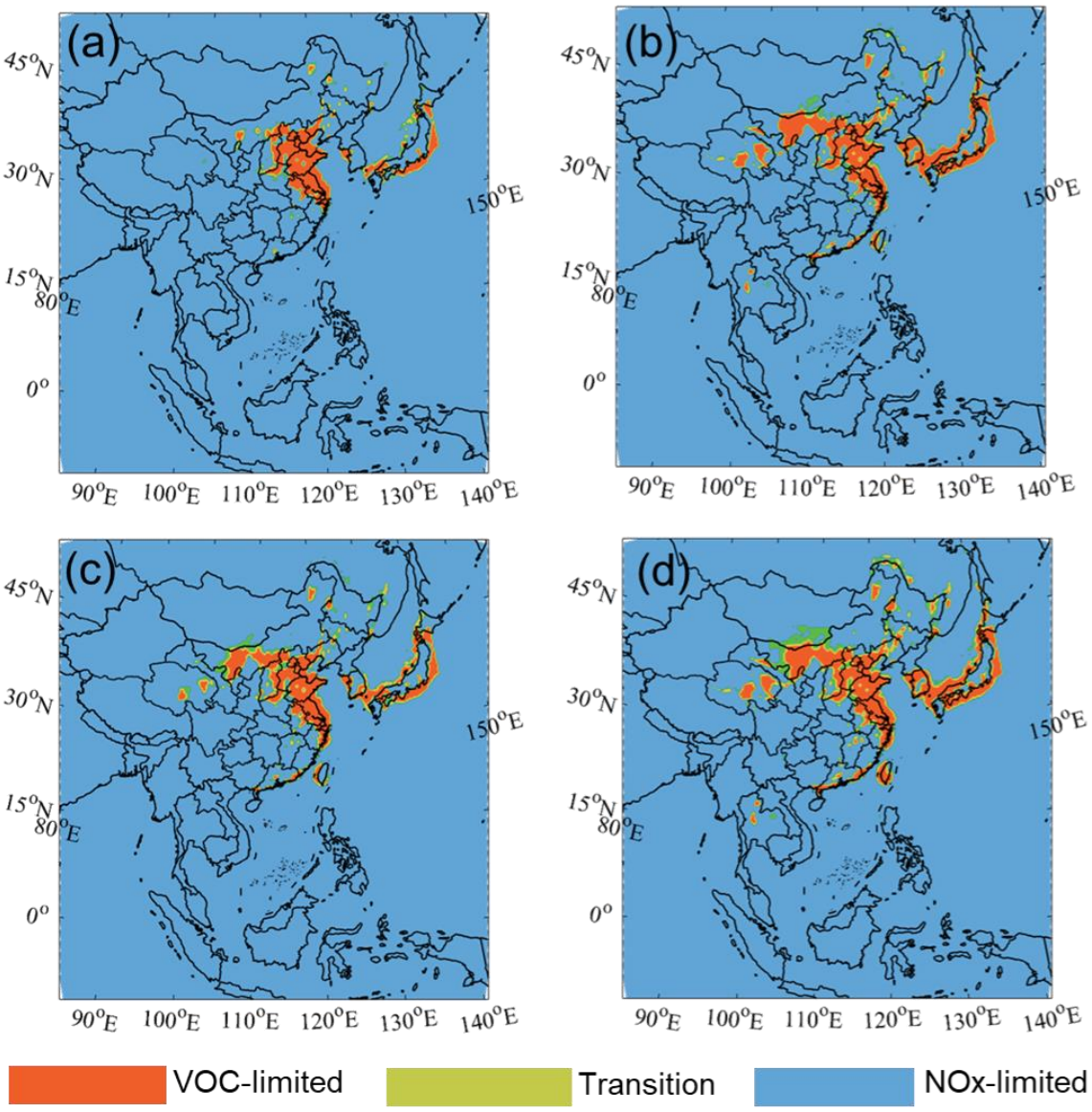

Figure 7: O_3 sensitivity regimes using (a) Def, (b) HONO, (c) Cl, and (d) Base cases. Classification of ozone sensitivity regime is based on production rates of H_2O_2 to HNO_3, and P_{H2O2}/P_{HNO3} of <0.06, 0.06 to 0.2, and >0.2 correspond to VOC-limited, transition, and NO_x-limited conditions, respectively (Zhang et al., 2009).

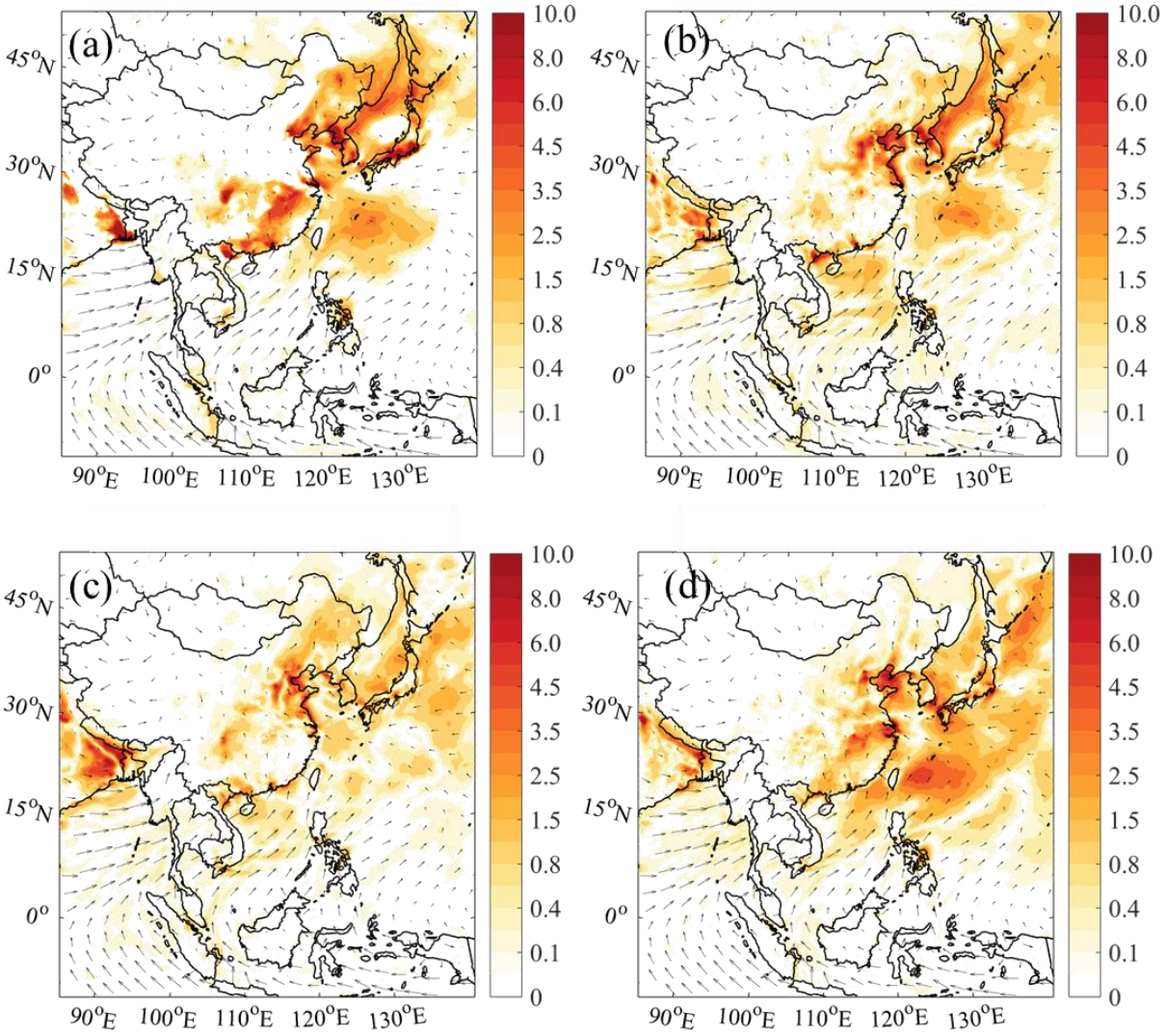

Figure 8: Averaged $PM_{2.5}$ enhancements due to ship emissions (Unit: μg m^{-3}) with (a) default chemistry (Def-Def_noship), (b) default and additional HONO chemistry (HONO-HONO_noship), (c) default and additional chlorine chemistry (Cl-Cl_noship), and (d) default and combined HONO and chlorine chemistry (BASE-BASE_noship). Arrows present simulated wind vectors from BASE case.

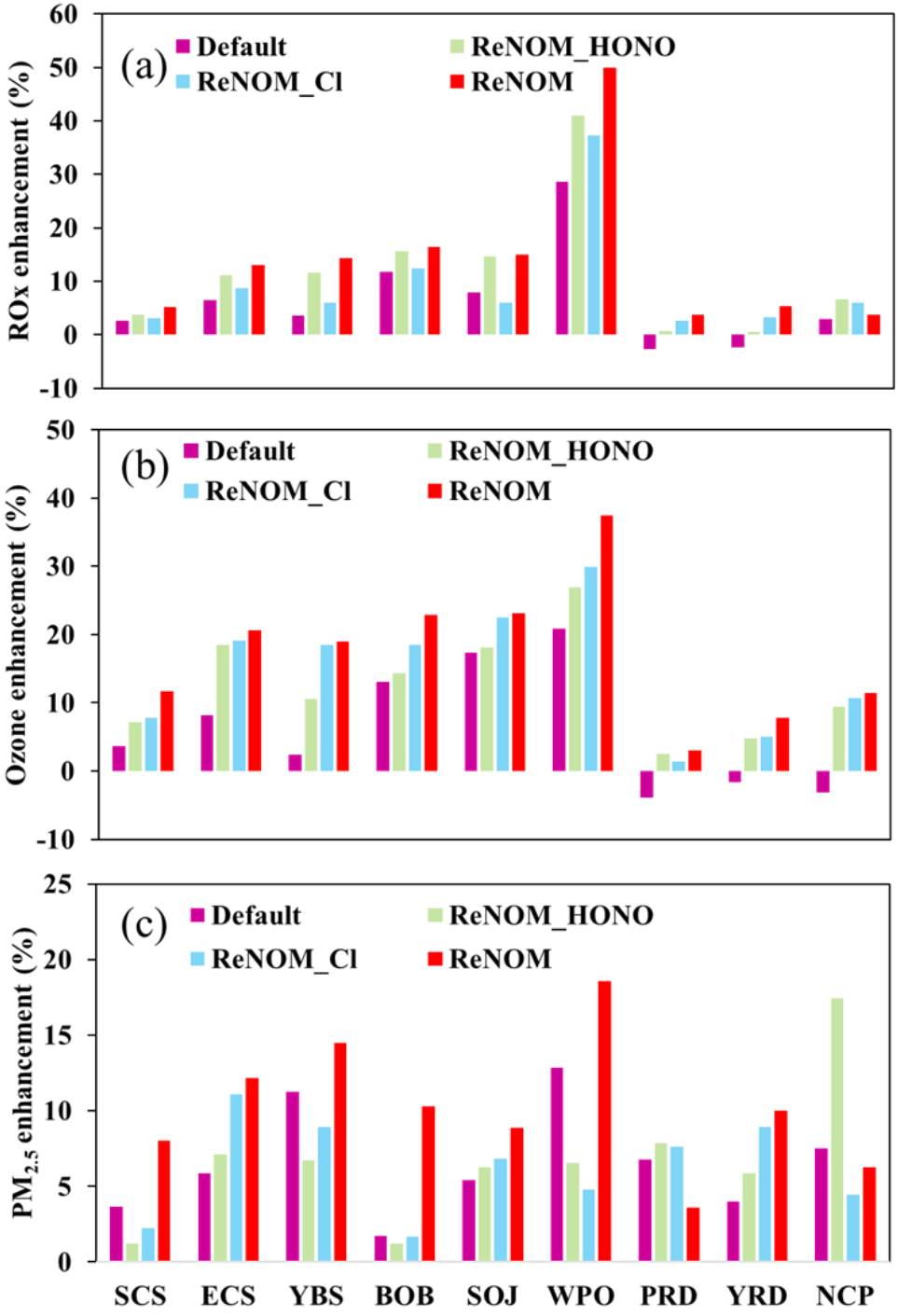

Figure 9: Contributions of ship emissions with different chemistry to average mixing ratios of (a) daytime RO_x, (b) ozone, and (c) $PM_{2.5}$ (with ship case (i.e., Def) – no ship case (i.e., Def_noship)) / with ship case (i.e., Def)).

650

Table 1: Experimental Setting

Cases	Anth Emis[a]	Ship Emis[b]	HONO Chem[c]	Chlorine Chem[d]
Def	Yes	Yes	No	No
Def_noship	Yes	No	No	No
Cl	Yes	Yes	No	Yes
Cl_noship	Yes	No	No	Yes
HONO	Yes	Yes	Yes	No
HONO_noship	Yes	No	Yes	No
BASE	Yes	Yes	Yes	Yes
BASE_noship	Yes	No	Yes	Yes

[a] Anthropogenic emissions except for ship emissions.

[b] Ship emissions except for directly emitted HONO.

[c] HONO chemistry.

[g] Chlorine chemistry.